Scientific Research Journal,
Vol 22, No 2 (2025) 151-172
https://doi.org/10.24191/srj.v22i2.31241

Effect of Different Preparation Approaches on Pt-Modified TiO_2/g-C_3N_4 for Effective Photocatalytic Degradation of RR4 Dye Under Visible Light

Rahil Azhar[1], Nurul Izzati Jahari[1], Nurul Izzah Roslan[1], Nur Syamimi Mohamad Abdul Adzis[1], Nur Hidayatul Syazwani Suhaimi[1], Nur Izzati Nabilah Zanal[1], Mohamad Afiq Rosli[1], Nor Azlian Abdul Manaf[2], Wan Izhan Nawawi Wan Ismail[1,*]

[1]Faculty of Applied Sciences, Universiti Teknologi MARA, Perlis Branch, Arau Campus, 02600 Arau, Perlis, Malaysia
[2]Physics Department, Centre for Defence Foundation Studies, National Defense University of Malaysia, Kem Sungai Besi, Kuala Lumpur, 57000, Malaysia

[*]Corresponding Author's E-mail:wi_nawawi@uitm.edu.my

Received: 03 October 2024
Accepted: 05 August 2025
Online First: 01 September 2025

ABSTRACT

This study investigates the effectiveness of TiO_2/g-C_3N_4/Pt composites prepared under different methods for photocatalytic dye degradation in wastewater. Initially, the TiO_2/g-C_3N_4 composite was prepared by dry and wet methods at different ratios. Both methods involved mixing P25 and g-C_3N_4, followed by calcination at 550 °C for 2 h with a heating rate of 5 °C/min in a tube furnace. To fabricate TiO_2/g-C_3N_4/Pt, platinum (Pt) was deposited onto the TiO_2/g-C_3N_4 wet composite using the photo deposition method. Reactive Red 4 (RR4) dyes were used as model pollutants to examine the photocatalytic activity of TiO_2/g-C_3N_4/Pt. The structural, optical, and photoelectrochemical properties of this prepared sample TiO_2/g-C_3N_4/Pt were further investigated in detail. Characterization was performed by X-ray diffraction (XRD), Fourier transform attenuated total reflectance (FTIR-ATR), and UV-vis diffuse reflectance spectroscopy (UV-Vis DRS). XRD analysis showed characteristic peaks at 13.2° and 27.3° for g-C_3N_4. In FTIR, functional groups present in TiO_2/g-C_3N_4/Pt (TC-Pt) were observed for NH_2 and OH around 3300 cm^{-1} to 3700 cm^{-1}, C-N at 1650 cm^{-1}, C=N at 1200 cm^{-1} and triazine ring at 801 cm^{-1}. Based on UV-Vis Analysis, TC-Pt shows a more absorption edge toward visible light, indicating a reduced

band gap from 2.80 eV to 1.6 eV. For PEC analysis, LSV, EIS, and CA demonstrated that TC-Pt has high current density under light, low charge transfer resistance under light, and high photocurrent response, respectively. For photocatalytic degradation, all modified samples degraded over 80% of RR4 dye within 1 h of light irradiation. Among the samples, TC-Pt with 1.5% Pt loading exhibits the highest degradation reaction rate constant with a value of 0.0708 min^{-1}.

Keywords: Wet; Dry; Photodeposition; Reactive Red 4 Dye; P25

INTRODUCTION

Water pollution is referred to as the contamination of water sources by poisonous substances that create water unsafe for human consumption and harmful to marine life. One of the biggest contributors to water contamination is the release of dye which is widely spread due to the operation of numerous textile and food industries [1]. The most used category of dyes in the textile industry is azo dyes [2]. Previous studies have found that azo dye can be harmful to organisms and cause mutation due to the presence of aromatic amine in the structure of azo dye [3]. Based on previous studies, many attempts to degrade this toxic dye in wastewater include chemical treatment [4], ion exchange [5], membrane filtration [6], and adsorption [7]. However, these techniques do not fully degrade textile dyes, and may generate unwanted intermediates [8].

According to Jalil et al. [3], heterogeneous photocatalysis has attracted significant interest due to its ability to degrade and mineralize dye pollutants. The efficiency of the photocatalyst starts from electrons on the metal's surface being excited by light irradiation moving from the valence band to the conduction band and forming an electron-hole pair [9]. Currently, titanium dioxide (TiO_2) is the most used semiconductor for photocatalytic degradation because of its excellent long-term photostability, low cost, and non-toxicity [10]. However, TiO_2 photocatalyst has some drawbacks such as a wide band gap, insufficient light absorption, and easy recombination of photogenerated carriers [11,12]. To address these issues, various modification methods have been developed to enhance the photocatalytic performance of TiO_2 such as doping with metals and nonmetals, coupling

with carbon-based materials, and introducing nanocomposites [13,14].

According to Karpuraranjith et al. [15], various materials have been combined or coupled with TiO_2 to create binary type II or Z-scheme heterojunctions such as molybdenum disulfide (MoS_2), copper oxide (Cu_2O), graphitic carbon nitride (g-C_3N_4), and silver bromide (AgBr). g-C_3N_4, a non-metal semiconductor is particularly suitable for coupling with TiO_2 due to its low band gap which allows it to absorb more visible light and thus enhance its photocatalytic activity [16]. However, this coupling still presents several limitations. These include rapid recombination of photogenerated electron-hole pairs, low specific surface area, and limited electrical conductivity which can lead to inefficient charge transfer. According to several studies, metallic additives, especially noble metals, have proven to be more effective in further improving the photocatalytic properties of TiO_2/g-C_3N_4 because of the synergistic effects between the metallic additives and TiO_2 [17,18]. Noble metal such as Ag, Au and Pt offer unique advantages when used as dopants due to strong localized surface plasmon effect (LSPR), enhanced visible light absorption, reduce the band gap and improved charge separation.

To address the gap in current research, this study presents a systematic comparison between dry and wet synthesis methods for preparing TiO_2/g-C_3N_4 composites. The novelty of this work lies in identifying how different preparation approaches influence dispersion, interfacial contact and overall photocatalytic performance. Furthermore, Pt was photodeposited onto the optimized TiO_2/g-C_3N_4 (from the wet method) to further enhance charge carrier separation and photocatalytic efficiency.

Hence in this study, TiO_2/g-C_3N_4 was synthesized through dry and wet methods. The wet method was chosen for doping TiO_2/g-C_3N_4 with Pt, to enhance photocatalytic degradation of reactive red 4 (RR4) dye performance. This work contributes a new perspective by linking synthesis strategy with performance outcomes in a Pt-modified Z-scheme heterojunction system. The aim of this study is to compare different synthesis methods (dry and wet) for TiO_2/g-C_3N_4 composites, identify the optimal preparation route, and enhance its photocatalytic activity through Pt modification. The photocatalytic performance of the resulting TiO_2/g-C_3N_4/Pt composite is evaluated for the degradation of RR4 dye under visible light.

EXPERIMENTAL METHODOLOGY

Chemicals and Materials

The chemicals used in this experiment are TiO_2-Degusa P25 (20% anatase, 80% rutile) obtained from Merck, Urea from Fluka, and RR4 dye (also known as Cibacron Brilliant Red) (Colour Index Number: 18105, λ_{max}: 517 nm) from Sigma-Aldrich. Distilled water was used to prepare all solutions. Microwave reactions were undertaken using a domestic microwave oven (Samsung ME711 K, 800 W, 2.45 GHz). Chemicals were used as received and reactions were performed under air.

Characterization Methods

Preparation of g-C_3N_4

The g-C_3N_4 was prepared by heating urea in a tube furnace. 15 g of urea was placed in a porcelain crucible and the sample was calcined in a muffle furnace for 550 ^oC for 2 h at a heating rate of 5 ^oC/min to obtain the g-C_3N_4 nanomaterials. After cooling at room temperature, the obtained g-C_3N_4 was ground using an agate mortar for further use.

Preparation of TiO_2/g-C_3N_4 with Different Method

The TiO_2/g-C_3N_4 (TC) composite was prepared using three different methods which are dry, wet, and in-situ method. The dry method involves mixing pre-synthesized commercially available TiO_2 (P25) with g-C_3N_4 to ensure a uniform distribution of the two components. In the wet method, the preparation is quite similar to the dry method but the prepared g-C_3N_4 and TiO_2 were physically mixed with the aid of a solvent for better interaction between the two materials. Meanwhile, the in-situ preparation involved preparing TC through the hydrothermal method using an autoclave.

Preparation of TiO_2/g-C_3N_4 via Dry Preparation

The first step in creating the heterojunction photocatalysts involved synthesizing pristine semiconductors pure of carbon nitride and titanium

dioxide. To prepare TC, a photocatalyst was synthesized through thermal heating using a muffle furnace with pre-prepared g-C_3N_4 and TiO_2 (P25). First, a specific mass ratio of P25 and g-C_3N_4 powders was thoroughly mixed and ground using an agate mortar and pestle for the physical blending. Then, the powder mixture was transferred to a crucible with a cover and calcinated at 550 °C for 2 h at a heating rate of 5 °C/min. After cooling the sample in the furnace, the resulting material was ground to obtain light yellow powder. Various mass ratios of P25 to g-C_3N_4 were explored, including 30:70, 50:50, 70:30, and 90:10. Based on the amount of P25 added in the obtained products g-C_3N_4 were labelled as, TC-70:30, TC-30:70, TC-50:50, TC-10:90, and TC- 90:10.

Preparation of TiO_2/g-C_3N_4 via Wet Method

In the wet preparation of TC, ethanol was used as a solvent to facilitate optimal interaction between TiO_2 and g-C_3N_4 . Initially, specific mass ratios of TiO_2 (P25) andg-C_3N_4 were thoroughly mixed with an agate mortar and pestle. Subsequently, the powder mixture was transferred to a crucible for the wet preparation paste. A sufficient amount of ethanol was added to the powder mixture in the crucible and mixed thoroughly until it formed a paste, ensuring an even distribution of the components. The sample was calcined in a tube furnace with a gradual heating rate of 5 °C/min up to 550 °C for 2 h. The resulting TC composite characterized by its light-yellow powder form, was allowed to cool in the furnace. Following this method, the TC was prepared with various mass ratios of P25 and g-C_3N_4 of 30:70, 50:50, 70:30, and 90:10, respectively which are labelled as TC-70:30, TC-30:70, TC-50:50, TC-10:90 and TC- 90:10.

Preparation of TiO_2/g-C_3N_4/Pt

To fabricate the TiO_2/g-C_3N_4/Pt (TC-Pt) catalyst, Pt (3%) was deposited onto the material using the photodeposition technique, utilizing chloroplatinic acid (H_2PtCl_6) as the precursor. Firstly, the distilled water, isopropyl alcohol (IPA), and chloroplatinic acid was placed in the Schlenk tube. The mixture solution was then bubbled with nitrogen gas for a few seconds to create degassing conditions. After that, the TC compound, previously prepared using the dry preparation was added to the Schlenk tube. Subsequently, the mixture was irradiated with a 250 W metal halide

lamp to simulate sunlight for 1 h while continuously stirring to obtain well-dispersed nanoparticles of Pt. After photodeposition, the suspension was isolated by washing it with distilled water several times and filtration. The washed residue was dried in an oven at 80 °C for 15 min. The TC-Pt sample was repeatedly synthesized by the same procedure but TC from the wet and in-situ methods was used instead of dry preparation. After the photodeposition of Pt, samples named TC-Pt (0.5), TC-Pt (1), and TC-Pt (1.5) were obtained by varying the amount of Pt used in the preparation process (0.5%, 1%, and 1.5).

Photocatalytic degradation of RR4 dye

The photocatalytic performance of TiO_2, g-C_3N_4 , TC and TC-Pt were examined for the degradation of RR4 dye under visible light irradiation. The photodegradation activity was carried out by suspending 0.03 g of photocatalyst in 25 mL of an aqueous 0.3 M solution of RR4 dye. The suspension was then poured into a glass cell of dimension 50 mm width × 10 depth × 80 height and irradiated with a 55 W fluorescent lamp. An aquarium pump model NS 7200 was used as an aeration source for oxygen supply. Throughout each photocatalytic experiment, the decolorization of RR4 was monitored at specific time intervals until either a steady state or complete decolorization was achieved. The absorbance was measured using a HACH DR 1900 spectrophotometer at 517 nm.

Photoelectrochemical Properties

Photoelectrochemical measurements, including linear sweep voltammetry (LSV), electrochemical impedance spectroscopy (EIS), chronoamperometry (CA), and Mott-Schottky (MS), were conducted using a CS310M Potentiostat/Galvanostat in a three-electrode setup with 0.5 M Na_2SO_4 as the electrolyte and a solar simulator (Cherusal TM-71, 50 Hz) as the light source. A platinum mesh and Ag/AgCl were used as the counter and reference electrodes, respectively. The working electrode was prepared by ultrasonically dispersing 10 mg of the catalyst in 200 μL of 95% ethanol, then spin-coated onto a 1 × 1 cm^2 FTO glass and dried overnight. LSV and EIS were performed under dark and illuminated conditions. LSV was recorded at 100 Hz with 0.5 mV intervals, CA with 30 s light on/off cycles, EIS in the 10^3–10^{-2} Hz range at 10 mV amplitude, and MS at 10,000 Hz. EIS was used

to examine an impedance characteristic of material, providing information about charge transfer resistance and electrochemical properties, which are usually illustrated by a Nyquist plot. The size or radius of the semicircles in the Nyquist plot is directly proportional to the charge transfer resistance. A smaller semicircle radius suggests lower charge transfer resistance, resulting in improved charge separation and faster transfer of electrons. All measurements were conducted at room temperature.

RESULTS AND DISCUSSION

XRD Analysis

The XRD patterns of TiO_2, g-C_3N_4 , TC 70:30 wet, TC 70:30 dry and TC-Pt (1.5), are presented in Figure 1 to observe the phase composition of the samples. The typical diffraction peaks corresponding to the anatase (JCPDS 21-1272) and rutile (JCPDS 21-1276) phases are observed in P25. The XRD spectrum of pure g-C_3N_4 exhibits two diffraction peaks at around 13.2° and 27.3°, which are indexed to the (100) crystal plane of tri-s-triazine repeating units and the (002) crystal planes of the hexagonal phase of g-C_3N_4 [19]. These peaks are in good agreement with the standard data for g-C_3N_4 as referenced in the Joint Committee on Powder Diffraction Standards (JCPDS) card No. 87-1526 [20]. The presence of these two-characteristic peaks in the XRD spectrum are consistent with literature report for g-C_3N_4 confirming that the synthesis sample is pure of g-C_3N_4.

In contrast, the XRD patterns of the TC 70:30 for wet and dry composites primarily show the diffraction peaks of TiO_2 while no distinct peaks corresponding tog-C_3N_4 are observed. This could be attributed to the lower crystallinity, poor range order, or relatively low content of g-C_3N_4 in the composite which often results in its signals being masked by the dominant TiO_2 peaks particularly at the 70:30 TiO_2/g-C_3N_4 ratio. Similar observations have been reported in previous studies where the g-C_3N_4 phase was undetectable in composites with low loading or poor crystallinity [21].

After Pt photodeposition, TC-Pt (1.5), no additional peaks corresponding to metallic Pt are detected which is likely due to the low Pt

loading and the high dispersion of small Pt nanoparticles that remain below the XRD detection threshold. The preservation of TiO_2's crystalline features and the absence of impurity peaks confirm the successful formation of the composite materials without altering their main phase structures.

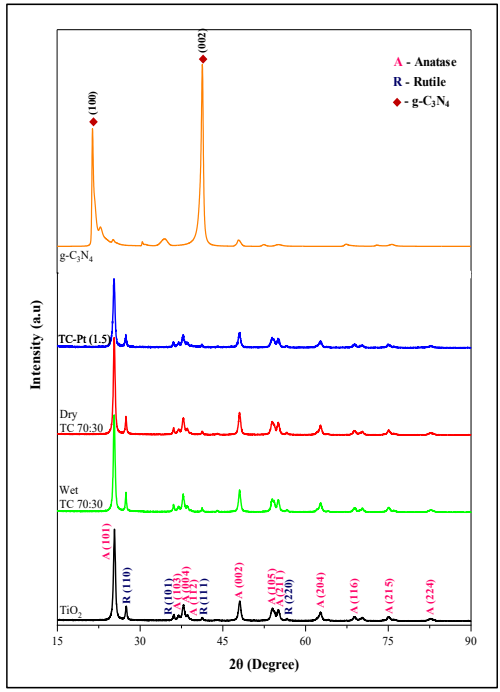

Figure 1: XRD spectra of TiO_2, g-C_3N_4, TC 70:30 wet, TC 70:30 dry and TC-Pt (1.5).

FTIR Analysis

To further analyze the functional groups and chemical bonding, Fourier Transform Infrared Spectroscopy (FTIR) was utilized by measuring the absorption of infrared radiation at different wavelengths for each sample. Figure 2 illustrates the FTIR spectra of (a) TC prepared by the wet method, (b) TC prepared by the dry method, and (c) Pt-modified TC (TC-Pt). The FTIR spectra of the TC samples prepared by both wet and dry methods exhibit characteristic absorption bands corresponding to both TiO_2 and g-C_3N_4 components indicating the successful synthesis of the composite material.

Figure 2 (a) and (b), shows the presence of a similar functional group for both wet and dry methods of TC. The identified functional groups include hydroxyl (-OH), amino (NH_2), imine (C=N), nitrile (C-N) and triazine ring. The peak between 3300 cm^{-1} and 3700 cm^{-1} corresponds to the O-H stretching vibrations on the surface hydroxyl groups and NH_2, while the peak between 1650 cm^{-1} and 1200 cm^{-1} is the typical vibration of g-C_3N_4 component and specifically attributed to the C-N and C=N stretching vibration [22, 23].

The broad band between 3000 cm^{-1} and 3700 cm^{-1} is likely resulting from O-H stretching vibrations of from the absorbed H_2O molecules. Additionally, the peaks around 810 cm^{-1} are related to the triazine ring of g-C_3N_4 [18]. Pure TiO_2 has a broad band in the 800-400 cm^{-1} range, is due to the Ti-O bond [24]. While both the wet and dry methods of TC have the same functional groups, there is a noticeable difference in the broadness of the peaks. It was observed in Figure 2 (a), that the O-H peak for the wet method is broader compared to the dry method in Figure 2 (b). The wet method shows a broader peak due to the addition of ethanol during the preparation of the wet sample, which results in more hydrogen bonding and absorption of water molecules.

According to Figure 2 (c), no obvious peaks corresponding to Pt can be observed in the spectrum, due to the small and low loading of Pt in each sample, which falls below the detection limit of FTIR. Moreover, Pt cannot be identified in the FTIR range up to 800 cm^{-1}. But Pt is most detected in the 500-800 cm^{-1} range, where its peak becomes more visible [25]. In summary, the FTIR analysis confirms the successful incorporation of TiO_2 and g-C_3N_4 in the composites prepared by both wet and dry methods, with noticeable differences in the extent of hydroxyl group presence and hydrogen bonding. The wet method appears to facilitate better dispersion and interaction of functional groups due to the addition of ethanol, which could enhance the photocatalytic properties of the composite. According to Nguyen *et al.* [26], ethanol is a polar protic solvent with low surface tension that helps reduce agglomeration and promotes a more uniform distribution of particles primarily due to improved surface interactions during the calcination stages. The low detectability of Pt in the FTIR spectra suggest the additional characterization is necessary to fully understand its distribution and impact on the composite's performance.

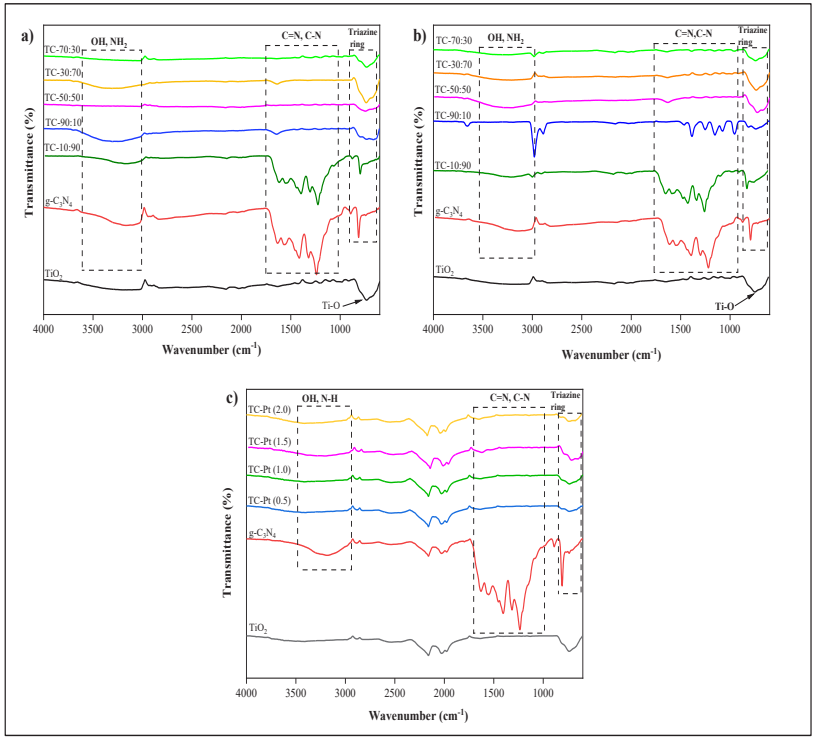

Figure 2: (a) FTIR Spectra of TC for wet method, (b) FTIR Spectra of TC for dry method and (c) FTIR Spectra of TC-Pt.

UV-Vis DRS

UV-Vis DRS analysis was used to investigate the optical properties of TC-70:30 for wet method and TC-Pt (1.5) samples. Figure 3 (a) and (b) show the absorption edge for TC-70:30 wet method and TC-Pt (1.5) sample and Tauc plot for determinations of the band gap, respectively. According to Figure 3 (a), the ternary TC-Pt (1.5) composite exhibited a red shift in the absorption edge after doped with Pt, which signifies the composite can respond more to visible light compared to TC-70:30. This red shift suggests enhanced visible light absorption which is beneficial for photocatalytic applications. In contrast, the TC-70:30 composite has significantly increased absorption capacity in the visible light area, indicating that composite

g-C_3N_4 and TiO_2 facilitate an expanded photo-responsive range [27-28]. Furthermore, the graph shows that the absorption capacity of TC-Pt (1.5) increases significantly in both the ultraviolet and visible light bands after the deposition of Pt NPs.

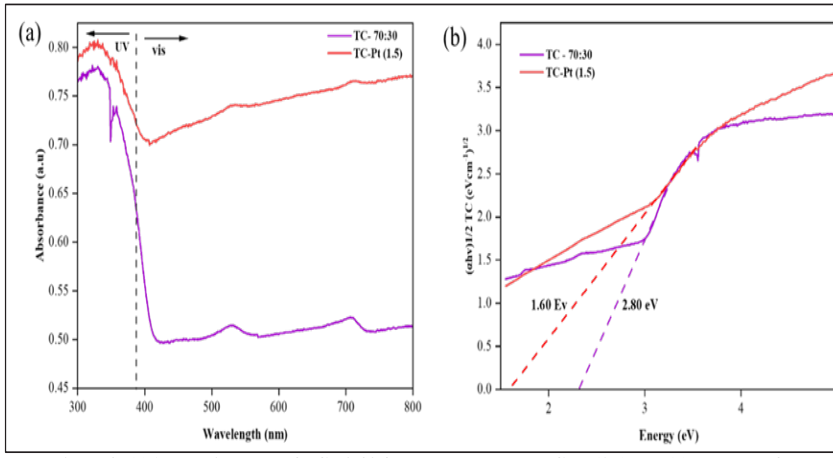

Figure 3: (a)Absorption edge of TC-70:30 for wet method and TC-Pt (1.5) and (b) Tauc plot for determinations of band gap.

The Tauc plot analysis of the UV-vis DRS data allows for the determination of the band gap energies of the composites. The band gap energy of the catalyst can be estimated from the Tauc plot using Eq. (1).

$$(\alpha h\nu)^2 = A\,(h\nu - Eg) \qquad (1)$$

Where α, v, h, E_g and A represent the absorption coefficient, light frequency, Plank's constant, respectively. As shown in Figure 3 (b), the band gaps of TC-70:30 for wet method and TC-Pt (1.5) samples were found to be 2.80 eV and 1.60 eV, respectively. The addition of Pt nanoparticles into the TC composite resulted in a significant reduction in the band gap from 2.80 eV to 1.60 eV. This decrease indicates that Pt modification effectively introduces energy levels within the composite structure, facilitating enhanced absorption of visible light. Consequently, this modification is expected to improve the photocatalytic activity of the TC-Pt (1.5) composite by extending its light absorption range into the visible spectrum which is crucial for efficient solar-driven photocatalysis.

Photoelectrochemical Analysis (PEC)

In this study, the photoelectrochemical analysis of TC-70:30 for wet method and TC-Pt (1.5) was evaluated using Linear Sweep Voltammetry (LSV) under both light and dark conditionals as shown in Figure 4 (a) and (b). LSV is used to measure the current response of an electrochemical system as the applied voltage is swept linearly over time. When the photocatalyst is exposed to light, it produces electron-hole pairs, which contribute to the photocurrent, as shown by an increase in current density in the LSV curves. In dark conditions, no light is present to excite the electrons in the photocatalyst. As a result, the measured current density is primarily owing to the material's inherent electrochemical activity, rather than photocatalytic contribution.

In Figure 4 (a), TC-70:30 shows an increase in current density with increasing potential under light, which reflects its ability to generate electron-hole pairs. Under dark conditions, the current density is much lower, indicating that photocatalytic activity only occurs in the presence of light. In Figure 4 (b), the LSV curve for TC-Pt (1.5) shows a higher current density under light than TC-70:30, demonstrating that Pt doping enhances photocatalytic activity. This is because Pt has high electrical conductivity, which helps in the effective separation of charge carriers by accepting electrons from TiO_2/g-C_3N_4, leading to increased photocatalytic efficiency [29].

Figure 4 (c) illustrates the Nyquist Plot for TC-70:30 wet method and TC-Pt (1.5). As shown in Figure 4, the blue curve of the TC-70:30 sample exhibits a larger semicircle radius than TC-Pt (1.5) (red curve), indicating higher resistance. Conversely, the TC-Pt (1.5) sample (red curve) has a smaller radius, indicating a lower charge transfer resistance. The presence of Pt doping in TC-Pt (1.5) increases the separation and transfer of photogenerated charge carriers (electrons and holes), resulting in a lower resistance. In contrast, Pt particles serve as electron traps, reducing the recombination of electron-hole pairs. As a result, according to the Nyquist plot, the TC-Pt (1.5) sample has better photocatalytic performance than the TC-70:30 sample. In Figure 4 (d) and (e), Chronoamperometry (CA) is a technique used in this analysis to measure the photocurrent response of the samples TC-70:30 wet method and TC-Pt (1.5) under constant

applied potential over time. Based on Figure 4 (d), the TC-70:30 of wet method sample shows a sharp initial decrease in photocurrent, followed by a sequence of smaller, more gradual peaks. This pattern illustrates that, while the material initially generates a considerable photocurrent due to electron excitation, photogenerated electron-hole pairs quickly recombine. This quick recombination limits overall photocurrent, indicating that the material's efficiency in charge separation is limited. Due to inefficient charge separation and high recombination rates, the TC-70:30 sample has a reduced photocurrent. In addition, Figure 4 (e) for the TC-Pt (1.5) sample shows an initial drop, but with more noticeable steps and a slightly higher total current than the TC-70:30 sample. The addition of Pt into TC-70:30 significantly increased transient photocurrent in TC-70:30, contributing to greater optical absorption and improved efficiency in photogenerated carrier separation and transfer [30].

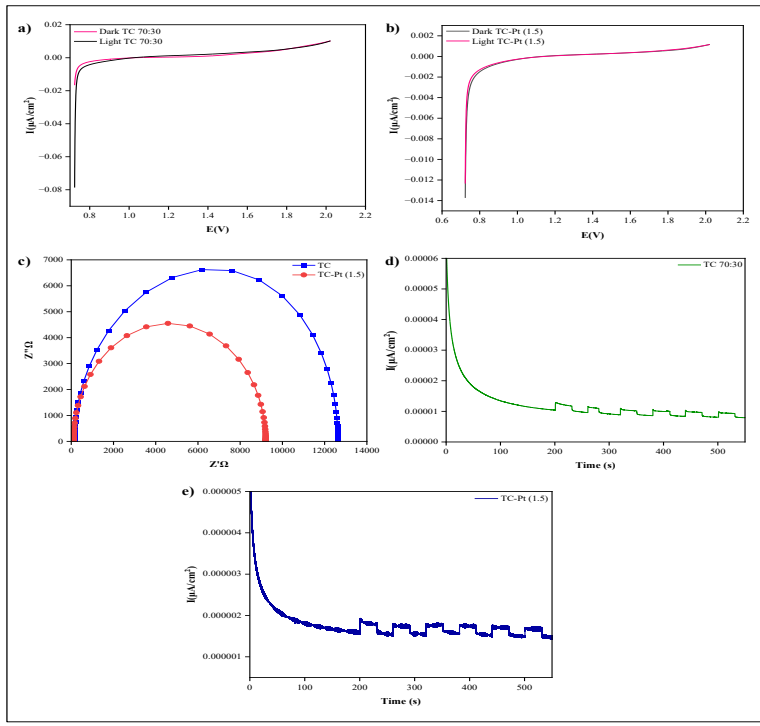

Figure 4: (a) LSV curve for TC-70:30 wet method, (b) LSV curve for TC-Pt (1.5), (c) Nyquist Plot for TC-70:30 wet method and TC-Pt (1.5), (d) Photocurrent response of TC-70:30 wet method and (e) Photocurrent response of TC-Pt (1.5).

Photocatalytic Degradation Study

Figure 5 illustrates the photocatalytic degradation of RR4 dyes for each method including wet, dry, and metal doping methods. Each line in the graph corresponds to a different sample composition of the photocatalyst, including TC-70:30, TC-30;70, TC-50:50, TC-10:90, and TC-90:10. The wet method in Figure 5 (a) demonstrates a more effective photodegradation process compared to the dry method in Figure 5 (c). For the wet method, the sample with a 70:30 ratio exhibits the highest degradation efficiency, reducing the percentage of remaining dye to below 10%. In contrast, the dry method for the same 70:30 ratio shows decreased efficiency because it required a longer time to achieve less than 10% remaining dye.

Furthermore, adding Pt to the TC composite significantly enhances the degradation efficiency of RR4 dye, as shown in Figure 5 (e). This improvement is attributed to Pt's ability to extend the light absorption range of TC, thereby enhancing photocatalytic efficiency under visible light. In addition, Figure 5 (b), (d), and (f) demonstrate that the photocatalytic degradation rate of all samples follows the pseudo-first order kinetics of the Langmuir-Hinshelwood model with R^2 values above 0.97.

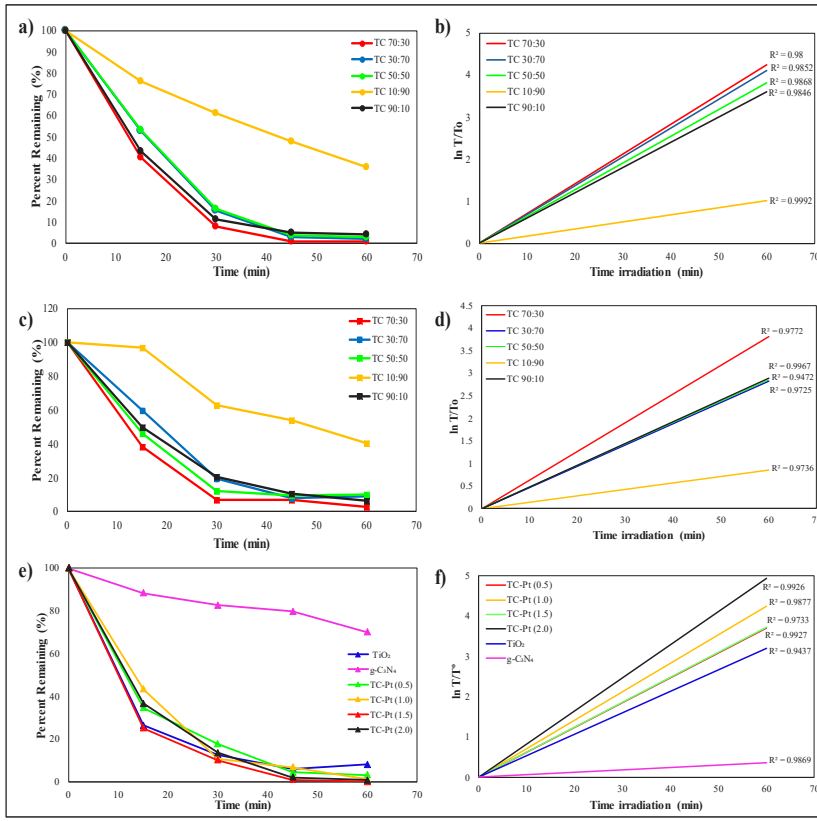

Figure 5: (a) Percentage remaining of RR4 dyes after photodegradation with TC for wet method, (b) Linear correlation for wet method of TC, (c) Percentage remaining of RR4 dyes after photodegradation process with TC for dry method, (d) Linear correlation for dry method of TC, (e) Percentage remaining of RR4 with TC-Pt and (f) Linear correlation for TC-Pt.

Figure 6 (a) illustrated k-value of photodegradation RR4 dyes for wet and dry method of TC and (b) k-value of photocatalytic degradation of RR4 dyes for TC-Pt. The apparent rate constant (k-value) was calculated using a pseudo-first-order kinetic model to provide insight into the degradation rate of RR4 dye. This parameter allows for a more precise comparison of catalytic activity by reflecting how quickly each sample facilitates dye degradation over time, even when final degradation efficiencies are similar. For every TC ratio tested, the wet method consistently results in higher k

values compared to the dry method as shown in Figure 6 (a). This indicates that the wet method is a suitable method to boost performance of coupling TC composites. During the wet preparation of TC, a solvent like ethanol is added to facilitate optimal interaction between TiO_2 and g-C_3N_4 particles, leading to a homogeneous mixture that maximizes the active sites available for photocatalytic reactions. The solvent allowed TiO_2 and g-C_3N_4 particles to come closer in contact and form heterojunction.

The highest rate constant observed is 0.0708 for the 70:30 ratio of TiO_2 to g-C_3N_4 using the wet method. This suggests that this specific ratio, when prepared using the wet method, provides the optimal balance of photocatalytic components, leading to maximum efficiency in degradation processes. The improved performance of the wet is likely due to the enhanced dispersion and interaction between the TiO_2 and g-C_3N_4 resulting in more efficient charge separation and transfer which are crucial for effective photocatalytic activity. Consequently, these findings emphasize the significance of the preparation method in improving the performance of TC composites.

Figure 6 (b) depicts the samples of TC-Pt (0.5), TC-Pt (1.0), and TC-Pt (1.5) which were prepared by varying the amounts of Pt (0.5%, 1%, and 1.5%, respectively). Introducing Pt forms a Schottky barrier at the interface with TiO_2 which helps trap electrons and prevent their recombination with holes. This effective charge separation leads to a higher generation of reactive species such as hydroxyl radicals and superoxide anions, which are crucial for the degradation of pollutants like RR4 dyes. Moreover, in the TC photocatalyst, g-C_3N_4 forms a heterojunction that further facilitates charge separation and transfer. The optimal sample, TC-Pt (1.5), exhibits the highest photocatalytic activity due to the balanced amount of g-C_3N_4 and the effective role of Pt in enhancing charge separation and reducing recombination rates. Consequently, these results underscore the importance of Pt doping and the synergistic effect of g-C_3N_4 in improving the photocatalytic performance of TC composites. TC-Pt (2.0) has not significantly increased.

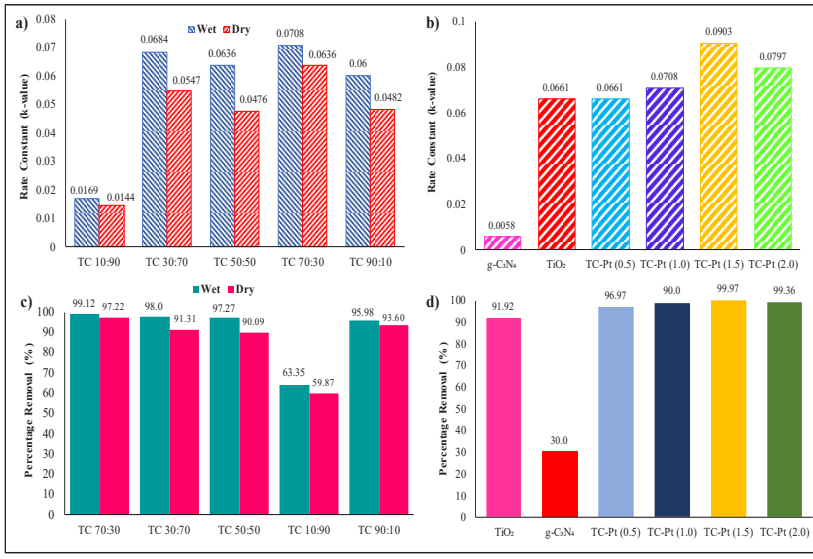

Figure 6: (a) k-value of photodegradation RR4 dyes for TC wet and dry method, (b) k-value of photocatalytic degradation of RR4 dyes for TC-Pt, (c) percentage removal for TC wet and dry and (d) percentage removal of TC-Pt.

CONCLUSION

XRD analysis confirmed the presence of anatase and rutile phases in TiO_2 and pure g-C_3N_4. In the 70:30 composites, g-C_3N_4 peaks were not visible, likely due to low crystallinity and content. No Pt peaks appeared after photodeposition, indicating successful dispersion without altering the TiO_2 structure. Comparing synthesis methods, the wet method significantly enhanced the photocatalytic activity of TC compared to the dry method, with the 70:30 ratio showing the best performance. Subsequent Pt doping via photodeposition further improved the activity, where TC-Pt (1.5) exhibited the highest degradation efficiency. UV-Vis DRS analysis showed enhanced visible light absorption and a reduced band gap (from 2.80 eV to 1.60 eV), while PEC measurements confirmed improved conductivity and charge transfer in the Pt-doped sample. Overall, the optimized TC-Pt (1.5) composite demonstrated excellent potential for visible-light-driven photocatalytic applications.

ACKNOWLEDGEMENTS

We would like to acknowledge Universiti Teknologi MARA (UiTM) for providing all the facilities. This work also was supported by the Ministry of Higher Education (MOHE) under fundamental Research Grant Scheme: FRGS/1/2022/STG04/UITM/02/1.

REFERENCES

[1] B. Lellis, C. Z. Fávaro-Polonio, J. A. Pamphile & J. C. Polônio, 2019. Effects of Textile Dyes on Health and The Environment and Bioremediation Potential of Living Organisms, *Biotechnology Research and Innovation*, 3(2), 275 - 290.

[2] B. J. Brüschweiler & C. Merlot, 2017. Azo Dyes in Clothing Textiles Can Be Cleaved into A Series of Mutagenic Aromatic Amines Which are Not Regulated Yet, *Regulatory Toxicology and Pharmacology,* 88, 214 - 226.

[3] A. A. Jalil, K. Ismail, M. A. M. Ishak, Z. Ahmad, S. Hamzah & W. Nawawi, 2020. Formation of an Amorphous Carbon Nitride/Titania Composite for Photocatalytic Degradation of RR4 Dye, *Journal of Water Process Engineering,* 35(24), 101209.

[4] S. Metin & D. İ. Çifçi, 2023. Chemical Industry Wastewater Treatment by Coagulation Combined with Fenton and Photo-Fenton Processes, *Journal of Chemical Technology and Biotechnology*, 98(5), 1158 - 1165.

[5] H. Ahmadpari & M. Taghavi, 2022. Application of Ion Exchange Technology in Water Treatment, *5th International Conference on Recent Innovations Chemistry and Chemical Engineering*, 16, 150264.

[6] E. O. Ezugbe & S. Rathilal, 2020. Membrane Technologies in Wastewater Treatment: A Review, *Membranes*, 10(5), 89.

[7] S. Satyam & S. Patra, 2024. Innovations And Challenges in Adsorption-Based Wastewater Remediation: A Comprehensive Review, Heliyon, 10(9), e29573.

[8] P. G. Ramos, J. Espinoza, L. A. Sánchez & J. Rodríguez, 2023. Enhanced Photocatalytic Degradation of Rhodamine B Employing Transition Metal (Fe, Cu, Co) Doped ZnO/RGO Nanostructures Synthesized by Electrospinning-Hydrothermal Technique, *Journal of Alloys and Compounds*, 966, 171559.

[9] S. Marimuthu, A. J. Antonisamy, S. Malayandi, K. Rajendran, P. Tsai, A. Pugazhendhi & V. K. Ponnusamy, 2020. Silver Nanoparticles in Dye Effluent Treatment: A Review on Synthesis, Treatment Methods, Mechanisms, Photocatalytic Degradation, Toxic Effects and Mitigation of Toxicity, *Journal of Photochemistry and Photobiology B-Biology,* 205, 111823.

[10] X. Zhang, S. Chen, X. Lian, S. Dong, H. Li & K. Xu, 2022. Efficient Activation of Peroxydisulfate by g-C_3N_4/Bi_2MoO_6 Nanocomposite for Enhanced Organic Pollutants Degradation Through Non-Radical Dominated Oxidation Processes, *Journal of Colloid and Interface Science,* 607, 684 - 697.

[11] S. Li, Z. Ying, R. Peng, Y. Zhou, S. Zhang, J. Zhao, S. Song, J. Chen & J. Ye, 2024. Enhanced 1,2-Dichloroethane Removal using g-C_3N_4/Blue TiO_2 Nanotube Array Photoanode in Microbial Photoelectrochemical Cells, *Chemosphere*, 363, 142839.

[12] X. Ma, H. Yang, B. Wang, L. Wu, M. Xue, Y. Li & H. Deng, 2023. Mechano-synthesized TiO_2/g-C_3N_4 Composites for Rapid Photocatalytic Removal of Perrhenate, *Journal of Environmental Chemical Engineering*, 11(2), 109423.

[13] M. Samadi, M. Zirak, A. Naseri, M. Kheirabadi & M. Ebrahimi, 2019. Design and Tailoring of One-Dimensional ZnO Nanomaterials for Photocatalytic Degradation of Organic Dyes: A Review, *Research on Chemical Intermediates,* 45(4), 2197 - 2254.

[14] S. Zarrin & F. Heshmatpour, 2018. Photocatalytic Activity of TiO_2/Nb_2O_5/PANI and TiO_2/Nb_2O_5/RGO As New Nanocomposites for Degradation of Organic Pollutants, *Journal of Hazardous Materials,* 351, 147 - 159.

[15] M. Karpuraranjith, Y. Chen, S. Rajaboopathi, K. Srinivas, D. Yang & B. Wang, 2022. Three-Dimensional Porous MoS_2 Nanobox Embedded g-C_3N_4@TiO_2 Architecture for Highly Efficient Photocatalytic Degradation of Organic Pollutant, *Journal of Colloid and Interface Science*, 605, 613 - 623.

[16] M. C. Herrera-Beurnio, F. J. López-Tenllado, J. Hidalgo-Carrillo, J. Martín-Gómez, R. Estévez, M. Castillo-Rodríguez, G. De Miguel, F. J. Urbano & A. Marinas, 2023. Controlled Photodeposition of Pt onto TiO_2-g-C_3N_4 Systems for Photocatalytic Hydrogen Production, *Catalysis Today*, 413 - 415, 113967.

[17] M. Ismael & Y. Wu, 2019. A Mini-Review on The Synthesis and Structural Modification of g-C_3N_4-Based Materials, And Their Applications in Solar Energy Conversion and Environmental Remediation, *Sustainable Energy & Fuels,* 3(11), 2907 - 2925.

[18] M. Sultana, A. T. M. A. I. Mondol, S. Islam, M. A. Khatun, M. Rahman, A. K., Chakraborty, M. S. Rahman, M. Rahman & A. S. Nur, 2023. Strategic Development of Metal Doped TiO_2 Photocatalysts for Enhanced Dye Degradation Activity Under UV–Vis Irradiation: A Review, *Current Research in Green and Sustainable Chemistry*, 7, 100383.

[19] Y. Huang, X. Xu, G. Fan, X. Zhu, L. Zhu & X. Chen, 2024. Effect of TiO_2 Crystal Phase on The Construction of TiO_2/g-C_3N_4 Heterojunction Photocatalyst for Efficient Sunlight Photodegradation of Naphthalene, *Colloids and Surfaces A: Physicochemical and Engineering Aspects,* 694, 134170.

[20] Y. Sun, J. He, D. Zhang, X. Wang, J. Zhao, R. Liu & F. Li, 2020. Simultaneous Construction of Dual-Site Phosphorus Modified g-C_3N_4 and Its Synergistic Mechanism for Enhanced Visible-Light

Photocatalytic Hydrogen Evolution, *Applied Surface Science,* 517, 146192.

[21] A. Balapure, M. M. Francis, H. Mude, P. A. Maroju, J. Ray Dutta & R. Ganesan, 2021. ZnO Core-Triggered Nitrogen-Deficient Carbonaceous g-C_3N_4 Shell Enhances the Visible-Light-Driven Disinfection, *Carbon Trends*, 5.

[22] S. Cao, Y. Zhang, K. Ding, J. Xu, Y. Zhao, Y. Wang, X. Xie & H. Wang, 2022. Efficient Visible Light Driven Degradation of Antibiotic Pollutants by Oxygen-Doped Graphitic Carbon Nitride Via the Homogeneous Supramolecular Assembly of Urea, *Environmental Research,* 210, 112920.

[23] Y. Lu, W. Wang, H. Cheng, H. Qiu, W. Sun, X. Fang, J. Zhu & Y. Zheng, 2022. Bamboo-Charcoal-Loaded Graphitic Carbon Nitride for Photocatalytic Hydrogen Evolution, *International Journal of Hydrogen Energy,* 47(6), 3733 - 3740.

[24] N. Arabi, A. Kianvash, A. Hajalilou, E. Abouzari-Lotf & V. Abbasi-Chianeh, 2020. A Facile and Green Synthetic Approach Toward Fabrication of Alcea- And Thyme-Stabilized TiO_2 Nanoparticles for Photocatalytic Applications, *Arabian Journal of Chemistry*, 13(1), 2132 - 2141.

[25] K. M. Batoo, K. H. Jassim, T. A. Qassem, S. Hussain, W. T. Hasson, S. S. Jalal, M. F. Ramadan, S. M. Hameed, A. H. Alawadi & A. Alsaalamy, 2024. Novel Magnetically Separable g-C_3N_4/TiO_2/$CuFe_2O_4$ Photocatalyst for Efficient Degradation of Tetracycline Under Visible Light Irradiation: Optimization of Process By RSM, *Journal of Saudi Chemical Society,* 28(3), 101871.

[26] P. A. Nguyen, T. K. A. Nguyen, D. Q. Dao & E. W. Shin, 2022. Ethanol Solvothermal Treatment on Graphitic Carbon Nitride Materials for Enhancing Photocatalytic Hydrogen Evolution Performance, *Nanomaterials,* 12(2), 179.

[27] F. Ge, Y. Chen, A. Liu, S. Guang & Z. Cai, 2019. Flexible and Recyclable SERS Substrate Fabricated by Decorated TiO_2 Film with Ag NPs on the Cotton Fabric, *Cellulose*, 26(4), 2689 - 2697.

[28] I. Khan, S. Khan, A. Zada, A. Ismail, M. I. A. Shah, M. Ateeq, P. Fazil, J. A. Khan, A. Khan, F. Jan, D. F. Shams, B. Miao, S. Ali & S. Wang, 2023. Suitable energy Avenue for The Dimension-Matched Cascade Charge Transfer Mechanism in A g-C_3N_4/TS-1 Heterostructure Co-Doped with Au–TiO_2 for Artificial Photosynthetic Green Fuel Production, *Catalysis Science & Technology*, 13(16), 4729 - 4743.

[29] Y. Su, L. Su, J. Ran, H. Yi & B. Liu, 2023. Biological Redox Cycling Amplification in A Self-Powered Photoelectrochemical Sensor Based on TiO_2/$CdIn_2S_4$/g-C_3N_4-WO_3 Photoanode for Sensitive Detection of Hg2+, *Analytica Chimica Acta,* 1263, 341279.

[30] B. Guo, C. Zhao, L. Zhou, Z. Yu, X. Liu, Z. Zhao & H. Yuan, 2022. Constructing A Novel Multi-Hierarchical TiO_2/g-C_3N_4/Ag-AgBr Photocatalyst with Dual Z-Scheme Heterojunction Utilizing Ag as The Charge Transfer Mediator, *Journal of Alloys and Compounds,* 900, 163514.